RESEARCH ARTICLE

An optical flow MTV based technique for measuring microfluidic flow in the presence of diffusion and Taylor dispersion

**Christoph S. Garbe · Karsten Roetmann ·
Volker Beushausen · Bernd Jähne**

Abstract A novel technique is presented for accurately measuring flow fields in microfluidic flows from molecular tagging velocimetry (MTV). Limited optical access is frequently encountered in microfluidic systems. Therefore, in this contribution we analyze the special case of tagging a line across the thin dimension of a microchannel and subsequent imaging along this line. This represents a set-up that is applicable to a wide range of microfluidic applications. A volume illumination has to be used, resulting in an integration of the visualized dye across the flow profile. This leads to the well-known effect of Taylor dispersion. Our novel technique consists of measuring motion from digital image sequences in a gradient-based approach. A motion model is developed which explicitly deals with brightness changes due to Taylor dispersion and additional molecular diffusion of dyes. The presented approach is specific to the case of a parabolic velocity profile. In the presence of these effects, an accurate computation of motion is only possible by applying this novel motion model. Our technique is tested on simulated sequences corrupted with varying levels of noise and on actual measurements. Measurements were conducted in a microfluidic mixer of precisely known flow properties. In the same mixer, a comparative study of our MTV technique to μPIV was performed. Also, the results were compared to bulk

measurements of the fluid flow velocity. The novel algorithm compared favorably and also, measurements were conducted on inhomogeneous flow configurations.

1 Introduction

Many high-performance separation techniques rely on flow of fluids through microchannels and can be used in applications such as high-pressure liquid chromatography (Desmet et al. 2006), capillary zone electrophoresis (Jorgenson and Lukacs 1983), and capillary electrokinetic chromatography (Terabe 1989). Technological progress in manufacturing microfluid components has led to a wide spreading of novel systems into diverse applications (Avram et al. 2006; Burns and Ramshaw 2001; Nguyen and Wereley 2006; Wang 2000; Eijkel and van den Berg 2005). In chemical and biochemical analytics, as well as in medical diagnostics, these novel devices can be used to speed up the analysis while only relying on minute probe volumes. This is due to the huge surface to volume ratio achieved by micro channels. In the future, microfluidic applications will increase in significance for chemical production processes. Here, boundary conditions can be controlled much more accurately and set accordingly. This leads to better controllable and thus more efficient reaction kinetics with less by-products. Current research is very active in microfluidic lab-on-a-chip applications (Burns and Ramshaw 2001; Stone et al. 2004), which are already hailed as a revolution in biological and medical sciences (Figeys and Pinto 2000).

The increase of interest in microfluidic devices directly leads to the need for diagnostic tools for the visualization and analysis of flow structures as well as mixture formation and reaction behavior directly inside the micro channels

C. S. Garbe (✉) · B. Jähne
Interdisciplinary Center for Scientific Computing,
University of Heidelberg, Heidelberg, Germany
e-mail: Christoph.Garbe@iwr.uni-heidelberg.de

B. Jähne
e-mail: Bernd.Jaehne@iwr.uni-heidelberg.de

K. Roetmann · V. Beushausen
Laser-Laboratorium Göttingen e.V, Göttingen, Germany

(Sinton 2004). More complex microfabricated fluid systems raise new issues of optimal fluid control such as the minimization of dead volumes, and the enhancement or retardation of scalar mixing. Here, non-destructive image-driven methods are preferable for various reasons.

Several different attempts have been made to image flows through microchannels. Basically, two approaches have emerged:

- micro particle imaging velocimetry (μPIV)
- molecular tagging velocimetry (MTV)

Taylor and Yeung (1993) were among the first to measure microchannel flow with particles. They seeded the flow with fluorescent latex microspheres. The motion was deduced from streaks obtained by illuminating the particles with continuous wave (cw) laser light for approximately 1 s. One major drawback Taylor and Yeung (1993) encountered with this technique of using dielectric particles as a tracer in electrokinetic liquid flows is the distinction between electroosmotic and electrophoretic forces acting on the particles. Furthermore, the local field gradients and fluid forces generated by polarizable or charged particles in a strong electric field also affect the motion of the tracer. Taylor and Yeung (1993) measured a small velocity deviation in the center of the capillary which they attributed to particle-induced viscous drag on the flow. Also, when using particle tracers, conditions in which there is a substantial velocity gradient across these particle have to be avoided. Otherwise, shear will lead to secondary motion. This prerequisite often leads to extremely small tracers. Such submicrometer particles essentially precludes the use of elastic scattering and requires the use of fluorescent particles, to achieve sufficient signal strength (Taylor and Yeung 1993). There are a number of applications in which the use of particles is prohibitive. For example, the flow through systems with a dense internal geometry such as packed columns cannot be measured in this way, since these particles will be effectively filtered out of the fluid. Another problem of the technique presented by Taylor and Yeung (1993) is that the velocity is computed from imaged streaks. This turns out to be limiting in terms of quantitative measurements as far as accuracy is concerned. Santiago et al. (1998) presented a μPIV technique that estimates motion from cross-correlation, similar to standard PIV techniques. This significantly increased accuracy and usability. Santiago et al. (1998) utilized an epifluorescent microscope, 100–300 nm diameter seed particles, and an intensified CCD camera to record high-resolution particle-image fields. A spatial resolution of $6.9 \times 6.9 \times 1.5$ μm was attainable. This technique was further improved by Olsen and Adrian (2000), who conducted diffusion measurements from μPIV. The diffusion is computed from a broadening of the correlation peak. A similar technique was used by Hohreiter et al. (2002) as a means of measuring temperature in microfluidic flows. Here, the diffusion caused by temperature due to Brownian motion (Brown 1828; Einstein 1905) is estimated from the correlation peak.

In order to avoid disadvantages associated with using particles for visualizing microfluidic flows, different dyes have been used as markers. These have been applied in fluid flow through capillaries as either a constant stream or as a plug of dye (Kuhr et al. 1993; Taylor and Yeung 1993; Tsuda et al. 1993). The usage of dyes as tracer is widespread in applications such as imaging of flow through gel-filled (Fujimoto et al. 1996), particle-packed, and open microchannel systems. Such techniques have also been applied to study the flows through micromachined channels on planar substrates and to evaluate different injection schemes for on-chip analysis and valveless pumping. Past implementations of this velocimetry approach include the use of photochromic molecules (LIPA, Chu et al. 1993; Falco and Chu 1988), excited-state oxygen fluorescence (RELIEF, Miles et al. 1987), specially engineered water-soluble phosphorescent molecules (Koochesfahani et al. 1993), and caged fluorescein (PHANTOMM, Koochesfahani and Nocera 2007). For an overview of the MTV technique, the reader is referred to (Koochesfahani 2000) for a compilation of applications and techniques, and to the recent manuscript (Koochesfahani and Nocera 2007) for details of caged dyes and exemplary applications. The scales on which measurements can be conducted range widely. Paul et al. (1998) have obtained quantitative velocity contours in pressure and electrokinetically driven flow through open capillaries of the order of 100 μm in diameter. Images of these measurements can be seen in Fig. 1. On larger scales, Dussaud et al. (1998)
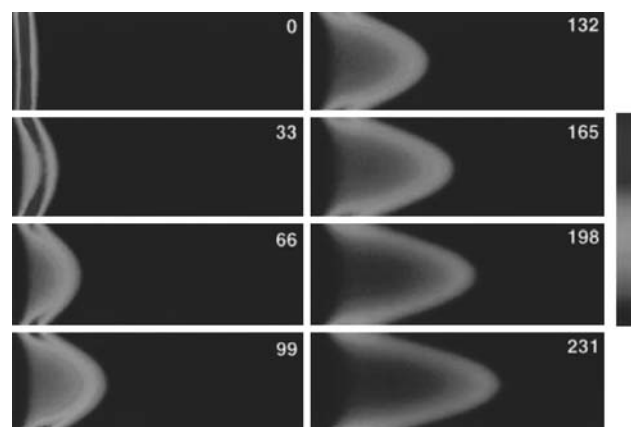

Fig. 1 Images of pressure-driven flow through an open 100 μm i.d. fused-silica capillary using a caged fluorescein dextran dye. The frames are numbered in ms as measured from the uncaging event. Reprinted with permission from Paul et al. (1998). Copyright 1998 American Chemical Society

utilized caged dyes to visualize the spreading of involatile and volatile surface films on water in a 16-cm diameter tank filled with a solution of caged fluorescein. Falco et al. (1993) and more recently Lempert and Harris (2000) compiled a review of efforts to measure flow velocities using molecular tagging. In the works of Miles et al. (1987), Lempert et al. (1995) and Lempert and Harris (2000), laser line tagging is used. In these techniques, a line is written to the fluid and the velocity is inferred from the displacement of the line centers. Due to the inherent aperture problem of such a pattern, only velocities normal to the line can be measured and no information can be retrieved from the tangential direction. Hill and Klewicki (1996) analyzed implications of measuring with such a pattern. Subsequently, they extended the line tagging technique to the use of a grid for marking the fluid (Hill and Klewicki 1996). Motion is estimated by locating the grid line centers using various techniques. The authors have reported the accuracy of this approach to ≈ 0.35 pixel RMS (Hill and Klewicki 1996). Gendrich and Koochesfahani (1996) and Gendrich et al. (1997) improved accuracy and implementation by estimation motion of the grid tagged fluid from spatial correlation (the authors quote an accuracy of 0.1 pixel for the 95% confidence level and 0.05 pixel RMS for a Gaussian distribution). This algorithm is similar to that employed for PIV techniques.

In microscopic settings, such as that encountered in microfluidic devices, optical access to the fluid is very limited. Due to experimental constraint, frequently a set-up is chosen in which the tagged lines are visualized along the optical axis of the imaging optics. A schematic drawing of this set-up is presented in Fig. 2. The experimental constraints lead to the need for volume illumination, similar to that often applied to μPIV (Meinhart et al. 2000). Since a light sheet cannot access the fluid orthogonal to the optical axis, integration of the visualized dye takes place along one dimension. This leads to a "smearing" of structures due to integration through depth. The effect is shown in Fig. 1, where dye is diffused into the areas behind the leading edge of the tagged line. The smearing of structures due to the integration with depth is commonly known as Taylor dispersion (Taylor 1954). On microfluidic scales, molecular diffusion leads to an additional smearing of the structures. These effects lead to inaccuracies in the techniques used previously.

In this contribution, we will introduce a novel technique for estimating microfluidic flow from MTV. This technique is specific to the case of a parabolic velocity profile. The effect of molecular diffusion and Taylor dispersion are explicitly modeled in the underlying motion model. This makes it feasible to measure velocities very accurately in the presence of these processes. The technique was first described by Garbe et al. (2006). Measurements were presented by Roetmann et al. (2006, 2007).

This paper is organized as follows: In Sect. 2 the effect of Taylor dispersion will be analyzed and the equation of motion resulting from the visualization process will be derived. The experimental set-up will be detailed in Sect. 3. The technique of estimation motion with the underlying motion model will be explained in Sect. 4. Results of the technique will be presented both on simulated and ground truth data in Sect. 5. This contribution concludes with Sect. 6.

2 Taylor dispersion

Taylor dispersion is an effect well known in microfluidics (Taylor 1954). Due to a parabolic flow profile, a

Fig. 2 A sketch of the experimental set-up of measuring microfluidic flows with caged dyes. On the right, a close up of the cross-section of the micro mixer is shown. The tagging is performed along the optical axis of the imaging system across the flow profile
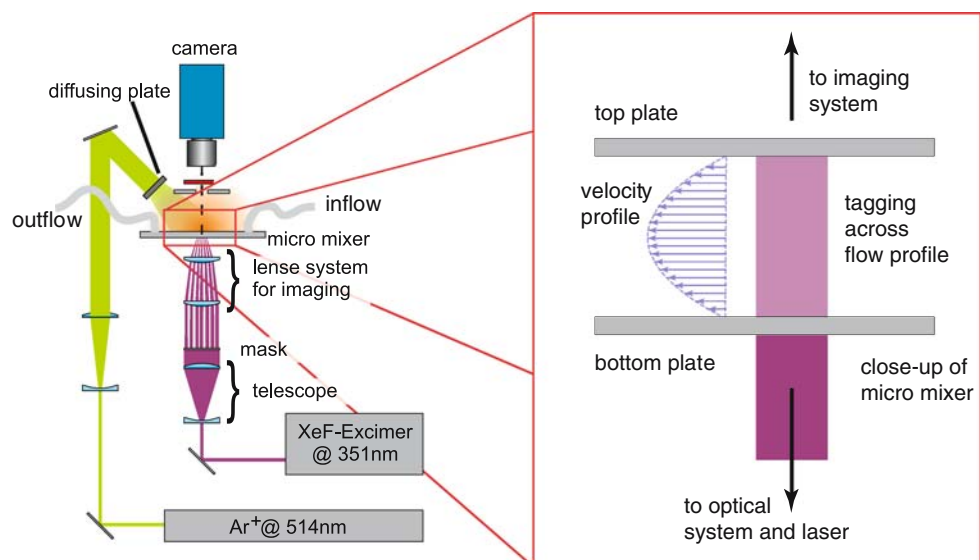
solute substance is dispersed along the flow volume. This effect can be seen in Fig. 1, where time steps of the spread of a marker in a flow through a capillary is shown. Due to the projection in visualizing the flow, the marker diffuses into the region behind the leading front, deformed by the parabolic flow profile. This deformation leads to different effects due to molecular diffusion orthogonal to the dominant flow direction (Beard 2001). In a number of microfluidic flows, one tries to minimize the effect of Taylor dispersion. This is achieved by channel geometry and by driving the fluid electrokinetically by electrophoresis or electroosmosis. Despite these efforts, a pressure gradient and hence the effect of Taylor dispersion can never be avoided completely (Dutta et al. 2001). Due to Taylor dispersion, previous techniques for estimating microfluidic flows from MTV encountered a number of difficulties, resulting in suboptimal performance. To resolve this problem, in this section an equation of motion is derived which explicitly models Taylor dispersion.

A viscous fluid driven by a pressure gradient between two stationary plates is also known as Poiseuille flow in the case of purely laminar flow. In the present application of microfluidic flows, the Reynolds number Re is in the range of $10 < Re < 100$. This makes it safe to assume that the flow can be described by the laminar flow of a Newtonian fluid. The velocity profile of a Poiseuille flow is given by (Kundu 1990)

$$u(z) = \frac{a}{2} z^2 - a \cdot b \cdot z \quad \text{with} \quad a = \frac{1}{\mu} \frac{dP}{dx}, \frac{dP}{dx} \le 0, \quad (1)$$

where $2b$ is the separation of the stationary plates, μ is the viscosity of the fluid and dP/dx is the pressure gradient along the direction of the flow. This type of flow and the associated quantities are visualized in Fig. 3a.

A marker such as a caged dye is introduced into the fluid and a pattern is written to the fluid at time $t = 0$. In later times, this structure is distorted by the paraboloid velocity profile developed by the Poiseuille flow. The two-dimensional cut of this process is shown for three time steps t_1–t_3 in Fig. 3a. Through this projection, the structure tagged in

the fluid is smeared in the direction of the fluid flow over time. This process, which might appear similar to anisotropic diffusion, is also known as *Taylor dispersion* (Taylor 1954). An image of this type of process can be seen in Fig. 4.

The marker is visualized through one of the plates, leading to an integration of the dye with respect to depth z. In the following, it is assumed that absorption across the depth of the microfluidic channel can be neglected. In our experiments, the penetration depth was generally a few orders of magnitude larger than the depth of the channel, warranting this assumption. Of course, when absorption cannot be neglected, Lambert-Beers's law can be incorporated, leading to more complex expressions (Garbe et al. 2007). As an initial condition, we assume that the flow is tagged at time $t = 0$. In the absence of absorption, the tagging is performed uniformly with depth. The width of the tagged structure is c. The integration across the depth of the channel results in

$$I = \int_{b \pm \sqrt{b^2 + \frac{2x}{at}}}^{b \pm \sqrt{b^2 + \frac{2(x+c)}{at}}} 1 \, dz$$

$$= \sqrt{\left\| b^2 + \frac{2 \cdot (c+x)}{a \cdot t} \right\|} - \sqrt{\left\| b^2 + \frac{2 \cdot x}{a \cdot t} \right\|}. \quad (2)$$

Here the integration limits are computed from Eq. (1) by integrating with respect to time and solving for z. I is the visualized image intensity and t is the time passed since tagging at $t = t_0$. x is the spatial coordinate taken along the flow direction. This analytic function is visualized in the sketch in Fig. 3b. This function can be developed into a Taylor series around $t = 0$, which results in

$$I = \sqrt{\frac{2}{t}} \left(\sqrt{\frac{c+x}{a}} - \sqrt{\frac{x}{a}} \right) + \frac{b^2 \sqrt{t}}{2\sqrt{2}} \left(\sqrt{\frac{a}{c+x}} - \sqrt{\frac{a}{x}} \right)$$
$$+ \mathcal{O}\left(t^{3/2} \right). \quad (3)$$

Differentiating the first term of the expansion in time leads to

Fig. 3 A sketch of the intensity profile of the dye for a Poiseuille flow at three times t_1–t_3 is shown in **a** together with the velocity profile $v(z)$. The projection of these profiles onto one plate as visualized by the camera is shown in **b**
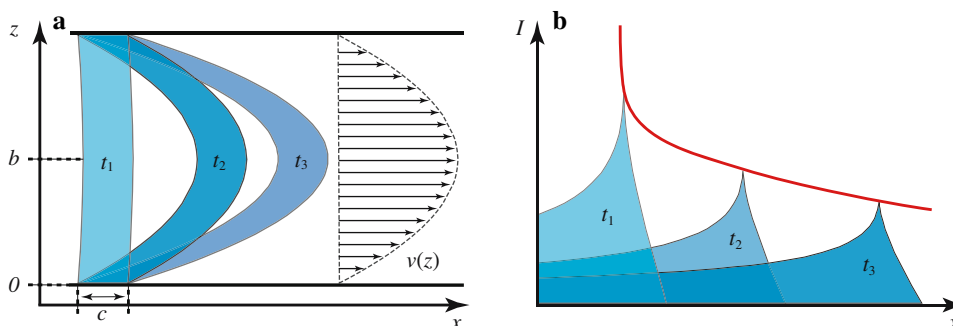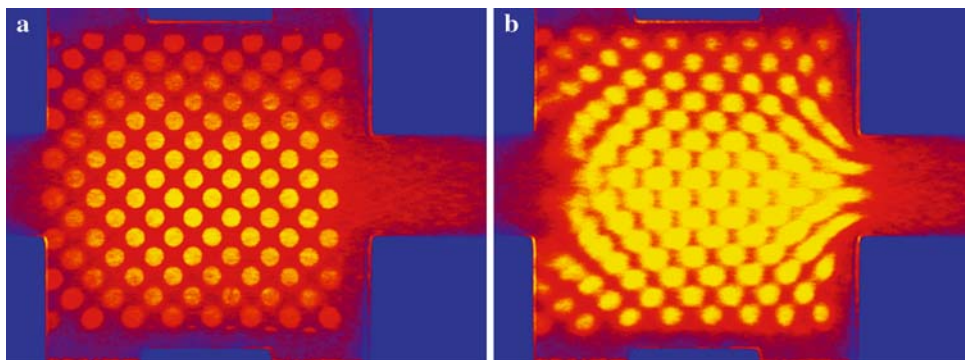
Fig. 4 In **a** and **b** two frames of a microfluidic image sequences are shown. The implication of Taylor dispersion can clearly be observed. Structures seem to diffuse in the direction of fluid flow. The intensities of **a** and **b** are scaled differently for better visibility

$$\frac{dI}{dt} = \frac{d}{dt}\left(\sqrt{\frac{2}{t}}\left(\sqrt{\frac{c+x}{a}} - \sqrt{\frac{x}{a}}\right)\right) = -\frac{1}{2t}I. \quad (4)$$

The velocity of the intensity structures subject to Taylor dispersion can thus be computed by solving the differential equation

$$\frac{dI}{dt} = u_1 \frac{\partial I}{\partial x} + u_2 \frac{\partial I}{\partial y} + \frac{\partial I}{\partial t} = -\frac{1}{2t}I. \quad (5)$$

Here u_1 and u_2 are the two-dimensional velocity components along the x and y direction. This linear differential equation can be rewritten in vector notation as

$$\frac{dI}{dt} = \mathbf{d}^\top \cdot \mathbf{p} = \left[\frac{1}{2t}I \ \frac{\partial I}{\partial x} \ \frac{\partial I}{\partial y} \ \frac{\partial I}{\partial t}\right] \cdot [1 \ u_1 \ u_2 \ 1]^\top = 0. \quad (6)$$

Here $\mathbf{d} = \left[\frac{1}{2t}I \ \frac{\partial I}{\partial x} \ \frac{\partial I}{\partial y} \ \frac{\partial I}{\partial t}\right]^\top$ represents the data vector and $\mathbf{p} = [1 \ u_1 \ u_2 \ 1]^\top$ is the parameter vector we try to recover subsequently using inverse theory. The transpose of a vector is denoted by $\top$.

Apart from Taylor dispersion, molecular diffusion is a dominant process in microfluidic flow visualization. This is due to the extremely small spatial extend of the fluidic structures and the resulting high local gradients. Combining the differential equation of Taylor dispersion and molecular diffusion ($dI/dt = D\Delta I$ with the Laplacian of intensities $\Delta I = \partial^2 I/\partial x^2 + \partial^2 I/\partial y^2$) leads to the following motion constraint equation

$$\begin{aligned}\frac{dI}{dt} &= d^\top \cdot p \\ &= \left[\frac{1}{2t}I - \left(\frac{\partial^2 I}{\partial x^2} + \frac{\partial^2 I}{\partial y^2}\right) \ \frac{\partial I}{\partial x} \ \frac{\partial I}{\partial y} \ \frac{\partial I}{\partial t}\right] \cdot [1 \ D \ u_1 \ u_2 \ 1]^\top = 0.\end{aligned} \quad (7)$$

Here D represents the diffusivity constant. It should be noted that here only a two dimensional, isotropic diffusion is assumed. This implies that diffusion with depth is taken to be negligible. It is obvious that this assumption is an oversimplification, since gradients with respect to z can be quite substantial in microfluidic flows subject to an parabolic flow profile. This is especially the case for long times

t relative to the mean velocity of the fluid. Since $\partial^2 I/\partial z^2$ cannot be measured directly, explicit assumptions concerning the initial intensity distribution have to be made in order to derived a closed form expression. The resulting equations are difficult to manage, even with these limiting assumptions. As will be shown later, the technique presented here is most suitable for short times t since uncaging the dyes. Therefore, inaccuracies due to the assumption of two-dimensional diffusion are negligible.

It should be noted that in deriving Eq. (6) and subsequently Eq. (7), it has been assumed explicitly that the flow is known à priori to have a parabolic profile, given by steady state Poiseuille flow. As it turns out (Garbe et al. 2007), any flow profile that can be approximated by an nth order polynomial of the type $u(z) = \alpha z^n$ leads to the constraint equation $dI/dt = -1/(n \cdot t) I$. This can be solved in a similar fashion as will be shown later for the case of Poiseuille flow. By treating the polynomial order n as a parameter, this makes it feasible to estimate the shape of the flow profile. Results of this technique will be presented in a subsequent publication. Therefore, this presented technique is not limited to polynomial flow profiles, although results will be presented for this type of flow, only.

3 Experimental set-up

The technique of measuring flow velocities of microfluidic flows presented in this work relies on caged dyes as markers of the flow. The tagging of the fluid is made possible through photo-chemical changes in the dye molecules. A schematic drawing of the experimental set-up is presented in Fig. 2. Details are found in Roetmann et al. (2005, 2006, 2007). Therefore, only a brief overview is given here.

Initially, the ability of fluorescence is deactivated by an additional functional group. Therefore, these dyes are also known as *caged dyes* (Gee et al. 2001). Intensive UV light can break up this functional group. Through an image

Fig. 5 Different mask used for writing intensity structures into the fluid
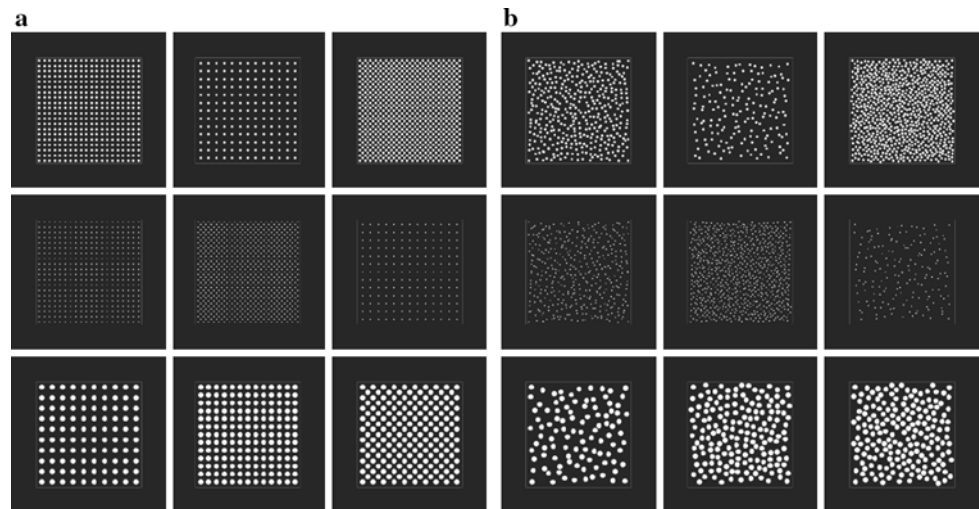
forming optical system, arbitrary two-dimensional patterns can be written to the fluid using a structured mask. The laser is homogeneously widened to illuminate the mask. A range of different patterns that were used in the context of this work are shown in Fig. 5. The pattern can be optimized depending on the flow velocity and on the properties of the flow to be inspected. Generally, bigger structures with further spacing in between are used for fast fluid flows and long measurement times. Smaller structures with little spacing deliver higher spatial resolution but are only viable for smaller velocities or shorter measurement time, as will be detailed later.

The patterns of dyes in the fluid are visualized with a second laser which is equally spatially homogeneously widened. The fluorescence is excited with an Argon Ionic Laser (Ar^+). The patterns in the fluid can be recorded both temporally and spatially highly resolved with a standard CCD camera.

The microfluidic flows are measured in a specially prepared chamber. The top and bottom boundary are made of quartz glass, which is highly transparent in the visible and UV spectrum. Two glass plates are separated with a metal plate by $2b = 200\ \mu m$. The width and depth of the

chamber is 5×5 mm. Different flow geometries can be realized from channels in the metal plate. These channels are connected to an array of 7 plugs which can be used for driving the flow with individual pressures and volume throughputs (Roetmann et al. 2007).

The set-up and visualization process leads to the following procedure: at time $t_0 = 0$, the fluid is tagged with the XeF Laser. The fluid inside the chamber is accessible non-invasively only through the glass plates on top and bottom of the Poiseuille flow. The beam of the laser writing the structured to the flow thus traverses through the whole depth of the fluid. A circular dot in the mask written to the fluid will thus lead to a cylindrical three-dimensional distribution of uncaged dyes. In later times, the parabolic velocity profile of plane Poiseuille flow distorts this three-dimensional cylinder. These transformed three-dimensional structures are projected onto the CCD chip of the imaging device. Great care is taken to align the camera orthogonal to the glass plate. Through this projection, the structure written to the fluid smeared in the direction of the fluid flow over time. This process can be modeled from Taylor dispersion using Eq. (7) also by taking isotropic diffusion into account. Images of such recordings for two

Fig. 6 A typical pattern written into a very simple microfluidic flow for calibration purposes in **a** and an inhomogeneous flow in **b**. The flow configuration in **a** is that of straight walls, well away from the inflow or outflow. In **b** the width of the channel changes, producing inhomogeneous flows
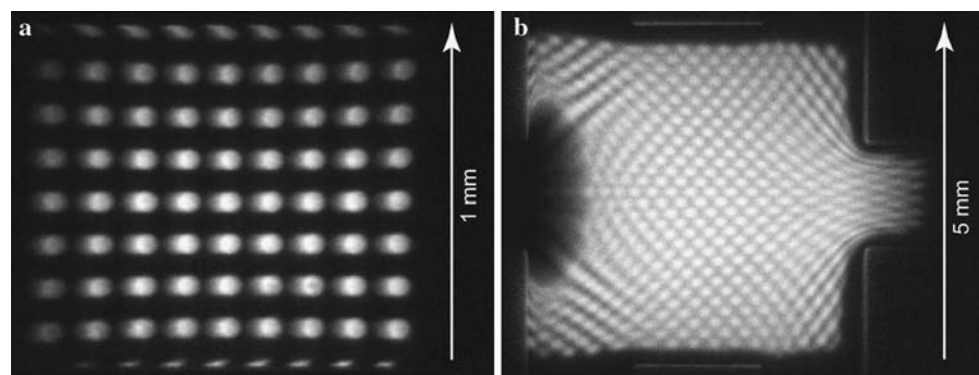
flow configurations are shown in Fig. 6. A more detailed account of the experimental set-up and measurement procedure can be found in Roetmann et al. (2007).

4 Motion estimation

The motion constraint equation derived for microfluidic flow with Taylor dispersion and isotropic diffusion is given by Eq. (7). This equation represents an ill-posed problem in the sense of Hadamar (1902). Only one constraint equation is given but three parameters are sought (the velocities in x and y direction and the diffusivity constant D). In order to estimate the full set of model parameters, additional constraints are required. These constraints can be constancy of parameters on a very local support in the sense of Lucas and Kanade (1981) or global smoothness as proposed by Horn and Schunk (1981). The problem of estimating microfluidic motion can thus be formulated in a local framework as presented by Garbe et al. (2003) with a robust extension such as the approach of Garbe and Jähne (2001). This local approach of motion estimation can be embedded in a global variational approach as shown by Spies and Garbe (2002) and Spies et al. (2004). A possible alternative uses a combined local global approach as proposed by Bruhn et al. (2005) which can also be extended to include brightness change models.

For the performance analysis presented here, dense flow fields are not of utmost importance. Therefore, a total least squares (TLS) approach, also known as structure tensor approach (Bigün and Granlund 1987; Bigün et al. 1991), is chosen. It should be noted that accuracy could be improved by employing a more elaborate approach at the cost of additional computing complexity. The technique of simultaneously estimating optical flow and change of image intensity is well known in literature (Haußecker and Fleet 2001; Haußecker et al. 1999; Negahdaripour and Yu 1993; Zhang and Herbert 1999). Details of the technique employed in the context of this paper have been explained previously (Garbe et al. 2003). Accuracy improvements were introduced in Garbe and Jähne (2001) and Garbe et al. (2002). Therefore, only a brief overview of the technique is presented below.

As derived in the previous section, we assume the image intensity I to change along trajectories according to Taylor dispersion and molecular diffusion. This is expressed by the total derivative dI/dt in Eq. (7). A commonly made assumption is that of a locally smooth motion field. Therefore, Eq. (7) can be pooled over a local neighborhood. This leads to an equation of type (7) for each pixel in the local neighborhood. Additionally, we require a weighting for the resulting overdetermined system of equations. This is introduced to weigh central pixels

stronger than those at the border of the neighborhood. The resulting system of equations is given by

$$\mathbf{WD}\cdot\mathbf{p}=\mathbf{W}\begin{bmatrix}\frac{1}{2t}I_1 & -\left(\frac{\partial^2 I_1}{\partial x^2}+\frac{\partial^2 I_1}{\partial y^2}\right) & \frac{\partial I_1}{\partial x} & \frac{\partial I_1}{\partial y} & \frac{\partial I_1}{\partial t}\\ \frac{1}{2t}I_2 & -\left(\frac{\partial^2 I_2}{\partial x^2}+\frac{\partial^2 I_2}{\partial y^2}\right) & \frac{\partial I_2}{\partial x} & \frac{\partial I_2}{\partial y} & \frac{\partial I_2}{\partial t}\\ \vdots & \vdots & \vdots & \vdots & \vdots\\ \frac{1}{2t}I_n & -\left(\frac{\partial^2 I_n}{\partial x^2}+\frac{\partial^2 I_n}{\partial y^2}\right) & \frac{\partial I_n}{\partial x} & \frac{\partial I_n}{\partial y} & \frac{\partial I_n}{\partial t}\end{bmatrix}$$
$$\cdot\begin{bmatrix}1\\ D\\ u_1\\ u_2\\ 1\end{bmatrix}$$
$$=0,\tag{8}$$

where $\mathbf{W}$ is a $n\times n$ diagonal weighting matrix, $\mathbf{D}$ is the $n\times 5$ data matrix and $\mathbf{p}$ is the sought parameter vectors. Subscripts I_i indicate the ith pixel in the local neighborhood. Depending on the noise in the data, typical neighborhoods are chosen to be 11×11 pixel, leading to a system of $n=121$ equations. The entries of the weighting matrix $\mathbf{W}$ are chosen by a two dimensional Gaussian distribution, centered at the center pixel. The spatio-temporal image intensity gradients $\partial I/\partial x$, $\partial I/\partial y$ and $\partial I/\partial t$ are computed from optimized Sobel filters (Jähne et al. 1999). Efficient implementations are available, significantly speeding up the estimation process. For instance, the weighting with $\mathbf{W}$ can be performed by convolving the gradient images $\partial I/\partial k$, $k\in x,y,t$ with a separable Gaussian blurring filter (Jähne 1997).

Equation (8) can be solved for the parameter $\mathbf{p}$ using a weighted total least squares approach (Van Huffel and Vandewalle 1991). This boils down to an eigensystem analysis of the square matrix $\mathbf{J}=\mathbf{W}^\top\mathbf{D}^\top\mathbf{DW}$, where $\mathbf{J}\in\mathbb{R}^{5\times 5}$ is also known as the extended structure tensor. The parameter vector $\mathbf{p}$ is then given as the normalized eigenvector to the smallest eigenvalue. This parameter vector is found for the pixel centered in the local neighborhood. The parameters for all pixels of the image sequence are computed by repeating this analysis for each pixel in a sliding window type fashion.

In this gradient-based approach, parameters can only be retrieved at locations where an intensity structure due to the uncaged dye is present. Otherwise $\partial I/\partial k$, $k\in x,y,t$ is equal to zero in Eq. (8). Therefore, a mask was computed by thresholding the gray-value of the images. Instead of performing the integration of the structure tensor with Gaussian smoothing filter, a normalized convolution (Granlund and Knutsson 1995; Knutsson and Westin 1993) with this mask was performed. This resulted in much more accurate estimates as compared to standard smoothing. In the case of convolving the gradient images with a Gaussian, wrong information (no motion) from areas without dye

diffuses into regions of dye concentration. This leads to a falsification and inaccurate estimates. The normalized convolution weights the smoothing with a certainty, which can be set to zero for areas without dye.

Also, by segmenting regions containing enough uncaged dye based on the image intensity, the computation of velocities are confined to the front of the smeared structure. This is seen by analyzing Fig. 3b. The regions of highest uncaged dye concentration are those with a low gradient of the fluid-flow profile, due to the longest integration length through the dye. These are the regions at the center of the flow (at $z = b$ half way in between the top and bottom plate). Proceeding in this fashion, the fluid-flow velocity computed are likewise those stemming from fluid parcels halfway between the two plates. The resulting estimated velocities are the maximum velocities v_{max} of the flow profile.

5 Results

In order to validate the presented algorithm, test measurements were performed. First, the basic applicability was tested on synthetic sequences. Here, an uncaged dye distribution with Gaussian cross section was modeled and transformed according to Taylor dispersion. Frames at different time steps of this test pattern are displayed in Fig. 7a. The test pattern was corrupted with normally distributed noise of varying standard deviation. Also different flow velocities were simulated. The results of these measurements is shown in Fig. 8a. The noise of current standard cameras is usually better than 0.9 gray-values. This means that the relative error expected is less than 2%. It should also be noted that the velocity computed is that of the center layer between the two plates as detailed in the

previous section. This corresponds to the maximum velocity of the profile. In the following, this maximum velocity v_{max} is the one that results from the novel technique are compared to.

In a second experiment on simulated data, the same measurement as with the Gaussian distribution were performed with two-dimensional sinusoidal patterns of different wavenumbers. Four time steps of one such simulated sequence are displayed in Fig. 7b. The results of these measurements are presented in Fig. 8b. The measured velocity oscillates around the true value with a slight bias to slow estimates. This is due to the fact that "uncaged dye structures" overlap. For the sinusoidal pattern, this happens almost immediately. The effect is sketched in Fig. 9. After a time $t = d/v_{max}$ the structures begin to overlap, where d is the initial distance between structures and v_{max} the maximum velocity in the center plane between the two plates. From the projected intensities in Fig. 9b it becomes clear that the intensity of the latter structure increases due to the added intensity of the former structure. Thus, the intensity changes are not correctly modeled by our present approach. In order to correctly estimate motion under these circumstances, this effect will have to be incorporated into the motion model. This extension is an area of future research. Currently, our novel technique is limited to situations were no such overlap occurs. This means that the measurement time $t = d/v_{max}$ has to be short enough. This is achieved by choosing the correct spacing d of tagged structures depending on the maximum expected velocity v_{max}.

Apart from measurements on simulated data, the technique was also tested on real world measurements with ground truth. The term ground truth is commonly used in remote sensing and digital image processing. It refers to measurements conducted by other means for comparison.

Fig. 7 Synthetic test sequences used for evaluating the proposed technique. In **a** a Gaussian pattern is written to the fluid and transformed according to Taylor diffusion, shown in **b** is the same for two-dimensional sinusoidal pattern. Flow motion directed from right to left along x axis. For each test sequence frame 1, 30, 60 and 150 are displayed. For display purposes frame 1 and 30 of **a** are scaled to overflow to be able to visualize all frames with the same gray value scaling
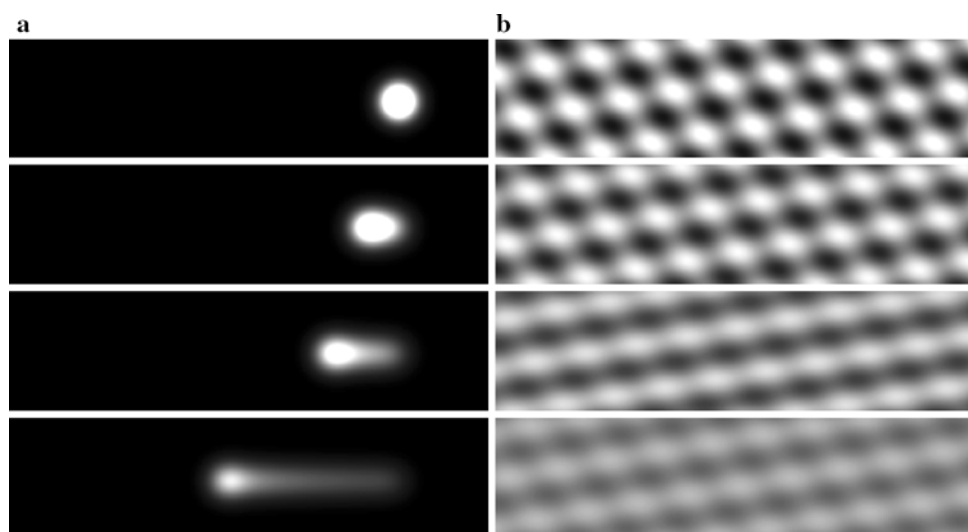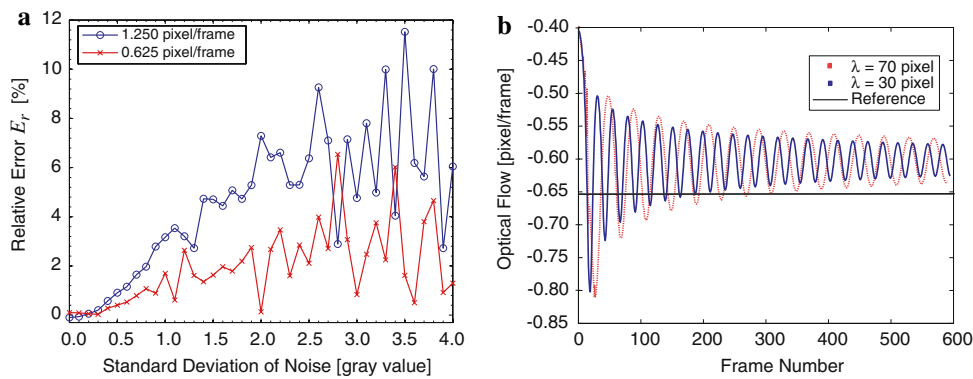
Fig. 8 **a** Relative error for the Gaussian test sequences with two different velocities (u_1 = 0.625 pixel/frame and u_2 = 1.25 pixel/frame) and varying noise levels. **b** Velocity of sine test sequences.

It is readily observed that the velocity undulates due to interferences of the sine pattern. These fluctuations are shown for two test patterns of different wavelengths λ. The true velocity is u = 0.625 pixel/frame

Fig. 9 Sketch of the effect of structure overlapping. In **a** the marked areas are transformed due to the parabolic flow profile. Two such structures separated by d overlap after time $t = d/v$. In **b** the corresponding projected intensities are shown
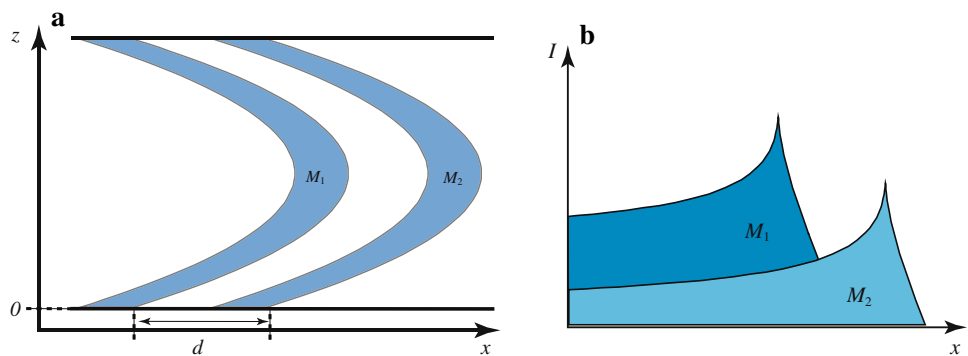
Like any measurements, the measurement of ground truth is corrupted by the measurement noise. However, usually one tries to minimize this error by employing highly accurate point measurements. However, one needs to be aware of the fact that the ground truth is based on an alternative measurement technique and thus also corrupted by measuring error.

In our case, we tried to minimize the measurement error by constructing a very simple geometry and performing measurements with precision instruments. These measurements were also combined with μPIV measurements to be able to compare our ground truth to an alternative, well-established technique. A purely laminar and parallel flow was adjusted to a number of different volume throughputs. The measurements were conducted well away from any flow disturbances such as changes in channel width. Generally, a flow profile can be considered to be fully developed for (Sigloch 2004)

$$\frac{L}{D_{\mathrm{h}}} \geq 0.06 Re, \tag{9}$$

where L is the distance from any flow disturbances, $D_{\mathrm{h}} = 4A/U$ is the hydraulic diameter, A is the cross sectional area and U is the wetted perimeter of the cross-section. Re is the Reynolds number of the flow. In our experiments, the

visualized area was much further away from any disturbances than L. Hence the profile is considered fully developed $< L$, the profile is not yet fully developed.

One frame of such a sequence is shown in Fig. 6a. The bulk flow velocities were measured accurately with a flow meter (SLG 1430, Sensirion). From knowledge of the geometry of the chamber (1.12 mm width and 0.2 mm depth), the centerline velocity v_{max} was computed. This centerline velocity v_{max} is referred to as ground truth in the following. The results from our extension of MTV were compared to this ground truth. A plot of this comparison is shown in Fig. 10. The data points from our new technique were measured by integrating over the center part of three consecutive frames. The standard deviation was computed over the same area of the three frames.

It can clearly be seen that there exists a good agreement between measurement and ground truth. The scatter in the measurements was found to be 6%. For most data points, the ground truth value is well within the error bar. However, some data points exhibit a bias to high values. A second experiment was performed using μPIV for measuring the centerline velocity. Details regarding this μPIV set-up can be found in Roetmann et al. (2007). The results of the comparisons of the μPIV measurements to the ground truth is also shown in Fig. 10. The same trend
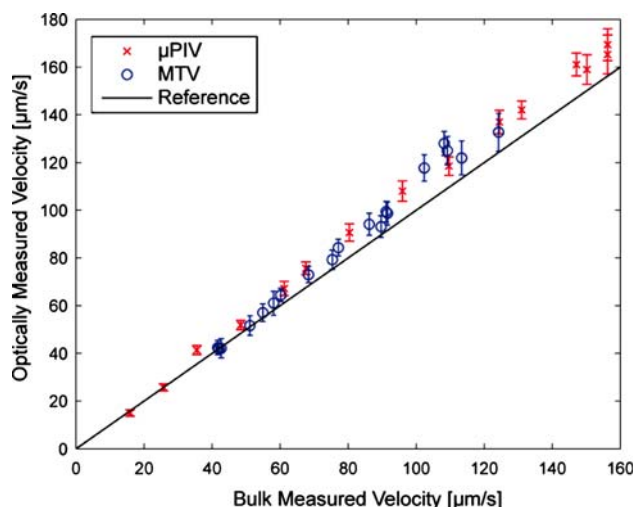
Fig. 10 Comparison of measured values from MTV (*blue circles*) and μPIV (*red crosses*) compared to ground truth measurement obtained from a flow meter (*solid black line*). Error bars were computed from deviations in the central part of three successive frames

observed with our MTV measurements is also persistent in the μPIV measurements. This leads to the conclusion that the reason for the bias can be found in the actual ground truth data. Although greatest experimental care was taken, it was impossible to produce a more accurate ground truth. This underlines the importance of non-invasive techniques for microfluidic flow measurements. The bias in the ground truth could have been evaded by performing concurrent measurements of MTV and μPIV. However, due to the optical set-up and limited optical access this was impossible to achieve. Therefore, both the MTV and μPIV measurements had to be conducted in succession, making a direct comparison of results unattainable. However, statistically both measurements of MTV and μPIV seem to agree quite well as is evident from Fig. 10. The error bars of both measurement techniques are roughly of the same magnitude, indicating that our new technique performs comparably to the well-established technique of μPIV.

This bias of the MTV results was also not detected on the synthetic test data, further pointing at the ground truth as the source for the bias. However, based on the simulations, the scatter in the data was higher than expected. The reason for the higher scatter might be due to fluctuations in the intensity of the readout laser. The optical flow based technique presented relies on the proposed motion model to accurately describe the spatio-temporal brightness changes of the acquired image sequences. Due to temporally and spatially inhomogeneous brightness fluctuations of the readout laser, this model is violated. In part, some fluctuations can be compensated by an adequate pre-processing. Still, not all fluctuations can be corrected in this way. These fluctuations, which are fast changing and spatially

inhomogeneous, will lead to a inaccuracies in the measured flow velocities. A more homogeneous illumination source, both temporally and spatially would lead to a drastic increase in accuracy.

The measurements presented previously on the homogeneous flow configuration are different to the actual demands of applications. Therefore, measurements were also performed on inhomogeneous flows. An image from such a flow is presented in Fig. 6b. The algorithm performed very well on these measurements. It should be noted that the stringent assumption of a parabolic flow profile no longer holds under these conditions. Nevertheless, results are more accurate than not modeling Taylor dispersion at all. Results are presented in Fig. 11. The qualitative picture corresponds very well to what is expected from this type of flow. Quantitative comparisons cannot be made due to the lack of ground truth. Results that are more accurate can be obtained by including nth order velocity profiles and estimating n, as indicated in Section 2. This extension of the technique will be analyzed and presented in a forthcoming publication.

6 Conclusion

In this contribution, a novel technique has been presented for measuring microfluidic flows by molecular tagging velocimetry (MTV). In contrast to current techniques, this method explicitly models Taylor dispersion (Taylor 1954) and molecular diffusion. Use is made of the assumption of a parabolic velocity profile, limiting the presented approach to this flow configuration. Extensions of this strict assumption are feasible as has been demonstrated by Garbe (2007). The motion parameters are computed by an optical flow technique. Isotropic diffusion is estimated concurrently with the motion models. This might make it possible to measure temperature spatially resolved in microfluidic
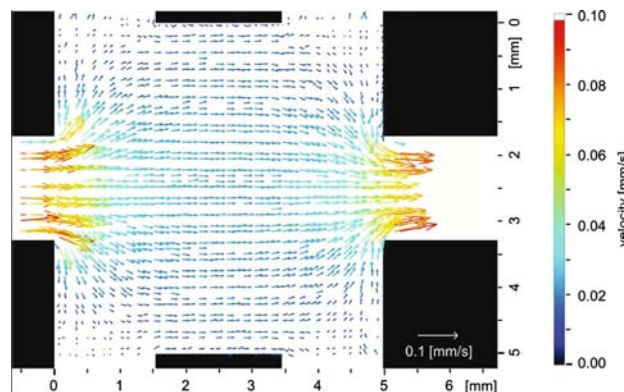

Fig. 11 The vector field computed for an inhomogeneous flow in the mixing chamber

flow. Such an extension of our technique is the subject of ongoing research.

The performance of the new technique has been analyzed on synthetic test sequences that were corrupted by varying noise. Furthermore, ground truth measurements have been conducted on a microfluidic channel with square geometry. In separate measurements, the results of our extension to MTV and μPIV were compared to actual bulk measurements of flow velocities. The measurements of our MTV technique agreed well with the μPIV measurements and the bulk flow measurements. The scatter in the measurements was found to be 6%. This scatter is in part due to spatio-temporal inhomogeneous fluctuations of the readout laser. The presented technique is prone to such intensity fluctuations. This is because fluid flow is measured from the recorded gray-values and spatio-temporal gradients thereof. Therefore, great experimental care should be taken to lessen or to eliminate intensity fluctuation of the readout laser. In our experiments, a reduction of these fluctuations was not possible due to the limited hardware availability. Still, the scatter in the measurements was comparable to those of μPIV. Our technique is thus comparable to this established measurement technique. It offers a novel technique that is highly applicable to problems inaccessible to μPIV.

References

Avram M, Avram A, Iliescu C (2006) Biodynamical analysis microfluidic system. Microelectron Eng 83(4–9):1688–1691

Beard DA (2001) Taylor dispersion of a solute in a microfluidic channel. J Appl Phys 89(8):4667–4669

Bigün J, Granlund GH (1987) Optimal orientation detection of linear symmetry. ICCV, London, pp 433–438

Bigün J, Granlund GH, Wiklund J (1991) Multidimensional orientation estimation with application to texture analysis and optical flow. IEEE Trans Pattern Anal Mach Intell 13(8):775–790

Brown R (1828) A brief account of microscopical observations made in the months of june, july and august, 1827, on the particles contained in the pollen of plants; and on the general existence of active molecules in organic and inorganic bodies. Philos Mag 4:161–173

Bruhn A, Weickert J, Schnörr C (2005) Lucas/kanade meets horn/schunck: combining local and global optic flow methods. Int J Comput Vis 61(3):211–231

Burns JR, Ramshaw C (2001) The intensification of rapid reactions in multiphase systems using slug flow in capillaries. Lab Chip 1(1):10–15

Chu CC, Wang CT, Hsieh CS (1993) An experimental investigation of vortex motions near surfaces. Phys Fluids A 5(3):662–676

Desmet G, Cabooter D, Gzil P, Verelst H, Mangelings D, Heyden YV, Clicq D (2006) Future of high pressure liquid chromatography: do we need porosity or do we need pressure? J Chromatogr A 1130(Spec.Iss.1):158–166

Dussaud AD, Troian SM, Harris SR (1998) Fluorescence visualization of a convective instability which modulates the spreading of volatile surface films. Phys Fluids 10(7):1588–1596

Dutta D, Leighton DT Jr. (2001) Dispersion reduction in pressure-driven flow through microetched channels. Anal Chem 73(3):504–513

Eijkel JCT, van den Berg A (2005) Nanofluidics: what is it and what can we expect from it? Microfluid Nanofluid 1(3):249–267

Einstein A (1905) Über die von der molekularkinetischen Theorie der Wärme geforderte Bewegung von in ruhenden Flüssigkeiten suspendierten Teilchen. Ann Phys 322(8):549–560

Falco RE, Chu CC (1988) Measurement of two-dimensional fluid dynamic quantities using a photochromic grid tracing technique. In: International Conference on Photomechanics and Speckle Metrology, vol 2. SPIE, San Diego, CA, pp. 706–710

Falco RE, Nocera DG, Rocco MC (1993) Quantitative multipoint measurements and visualization of dense liquid–solid flows using laser induced photochemical anemometry (lipa). In: Particulate two-phase flow. Butterworth-Heinemann, pp. 59–126

Figeys D, Pinto D (2000) Lab-on-a-chip: a revolution in biological and medical sciences. Anal Chem 72(9):330A–335A

Fujimoto C, Fujise Y, Matsuzawa E (1996) Fritless packed columns for capillary electrochromatography: separation of uncharged compounds on hydrophobic hydrogels. Anal Chem 68(17):2753–2757

Garbe CS (2007) Fluid flow estimation through integration of physical flow configurations. In: Hamprecht F, Schnörr C, Jähne B (eds) Pattern recognition, vol LNCS 4713. Springer, Heidelberg, pp 92–101

Garbe CS, Jähne B (2001) Reliable estimates of the sea surface heat flux from image sequences. In: Radig B (ed) Mustererkennung 2001, 23. DAGM Symposium, München, LNCS Lecture notes on computer science. Springer, Heidelberg, pp. 194–201

Garbe CS, Spies H, Jähne B (2002) Mixed ols-tls for the estimation of dynamic processes with a linear source term. In: Van Gool L (ed) Pattern Recognition, Lecture Notes in Computer Science, vol LNCS 2449. Springer, Zurich, pp. 463–471

Garbe CS, Spies H, Jähne B (2003) Estimation of surface flow and net heat flux from infrared image sequences. J Math Imaging Vis 19(3):159–174

Garbe CS, Roetmann K, Jähne B (2006) An optical flow based technique for the non-invasive measurement of microfluidic flows. In: 12th International symposium on flow visualization, Göttingen, Germany, pp. 1–10

Garbe CS, Degreif K, Jähne B (2007) Estimating the viscous shear stress at the water surface from active thermography. In: Garbe CS, Handler RA, Jähne B (eds) Transport at the air sea interface—measurements, models and parametrizations. Springer, Berlin, pp. 223–239

Garbe CS, Pieruschka R, Schurr U (2007) Thermographic measurements of xylem flow in plant leaves. New phytologist (Submitted)

Gee KR, Weinberg ES, Kozlowski DJ (2001) Caged q-rhodamine dextran: a new photoactivated fluorescent tracer. Bioorg Med Chem Lett 11(16):2181–2183

Gendrich CP, Koochesfahani MM (1996) A spatial correlation technique for estimating velocity fields using molecular tagging velocimetry (mtv). Exp Fluids 22(1):67–77

Gendrich CP, Koochesfahani MM, Nocera DG (1997) Molecular tagging velocimetry and other novel applications of a new phosphorescent supramolecule. Exp Fluids 23(5):361–372

Granlund GH, Knutsson H (1995) Signal processing for computer vision. Kluwer, Dordrecht

Hadamar J (1902) Sur les problèmes aux dérivées partielles et leur signification physique. Princeton Univ Bull, pp. 49–52

Haußecker H, Fleet DJ (2001) Computing optical flow with physical models of brightness variation. PAMI 23(6):661–673

Haußecker H, Garbe C, Spies H, Jähne B (1999) A total least squares framework for low-level analysis of dynamic scenes and processes. In: DAGM. Springer, Berlin, pp. 240–249

Hill RB, Klewicki JC (1996) Data reduction methods for flow tagging velocity measurements. Exp Fluids 20(3):142–152

Hohreiter V, Wereley ST, Olsen MG, Chung JN (2002) Cross-correlation analysis for temperature measurement. Meas Sci Technol 13(7):1072–1078

Horn BKP, Schunk B (1981) Determining optical flow. Artif Intell 17:185–204

Jähne B (1997) Digital image processing, 4th edn. Springer, Berlin

Jähne B, Scharr H, Körkel S (1999) Principles of filter design. In: Jähne B, Haußecker H, Geißler P (eds) Handbook of computer vision and applications, vol 2. Academic Press, London, pp. 125–151

Jorgenson JW, Lukacs KD (1983) Capillary zone electrophoresis. Science 222(4621):266–272

Knutsson H, Westin CF (1993) Normalized and differential convolution: methods for interpolation and filtering of incomplete and uncertain data. In: CVPR. New York, pp. 515–516

Koochesfahani MM (ed) (2000) Molecular tagging velocimetry. Meas Sci Technol 11(9):1235–1300

Koochesfahani MM, Nocera DG (2007) Molecular tagging velocimetry. In: Tropea C, Yarin A, Foss J (eds) Springer handbook of experimental fluid mechanics, vol B. Springer, Berlin, pp 362–382

Koochesfahani MM, Gendrich CP, Nocera DG (1993) A new technique for studying the lagrangian evolution of mixing interfaces in water flows. Bull Am Phy Soc 38:2287

Kuhr WG, Licklider L, Amankwa L (1993) Imaging of electrophoretic flow across a capillary junction. Anal Chem 65(3):277–282

Kundu PK (1990) Fluid mechanics. Academic, San Diego

Lempert WR, Harris SR (2000) Flow tagging velocimetry using caged dye photo-activated fluorophores. Meas Sci Technol 11(9):1251–1258

Lempert WR, Ronney P, Magee K, Gee KR, Haugland RP (1995) Flow tagging velocimetry in incompressible flow using photo-activated nonintrusive tracking of molecular motion (PHAN-TOMM). Exp Fluids 18(4):249–257

Lucas B, Kanade T (1981) An iterative image registration technique with an application to stereo vision. In: DARPA image understanding workshop, pp. 121–130

Meinhart CD, Wereley ST, Gray MHB (2000) Volume illumination for two-dimensional particle image velocimetry. Meas Sci Technol 11:809–814

Miles R, Cohen C, Connors J, Howard P, Huang S (1987) Velocity measurements by vibrational tagging and fluorescent probing of oxygen. Opt Lett 12:861–863

Negahdaripour S, Yu CH (1993) A generalized brightness chane model for computing optical flow. In: International conference in computer vision, Berlin, pp. 2–7

Nguyen NT, Wereley ST (2006) Fundamentals and applications of microfluidics, 2nd Edition. Artech House Publishers

Olsen MG, Adrian RJ (2000) Out-of-focus effects on particle image visibility and correlation in microscopic particle image velocimetry. Exp Fluids 29(7):166–174

Paul PH, Garguilo MG, Rakestraw DJ (1998) Imaging of pressure- and electrokinetically driven flows through open capillaries. Anal Chem 70(13):2459–2467

Roetmann K, Garbe CS, Beushausen V (2005) 2d-molecular Tagging Velocimetry zur Analyse Mikrofluidischer Strömungen. In: Tagungsband Lasermethoden in der Strömungsmesstechnik (GALA), pp. 26/1–26/10

Roetmann K, Garbe CS, Schmunk W, Beushausen V (2006) Micro-flow analysis by molecular tagging velocimetry and planar raman-scattering. In: Proceedings of 12th International symposium on flow visualization, Göttingen, Germany

Roetmann K, Schmunk W, Garbe CS, Beushausen V (2007) Micro-flow analysis by molecular tagging velocimetry and planar raman-scattering. Exp Fluids. doi:10.1007/s00348-007-0420-1

Santiago JG, Wereley ST, Meinhart CD, Beebe DJ, Adrian RJ (1998) A particle image velocimetry system for microfluidics. Exp Fluids 25(4):316–319

Sigloch H (2004) Technische Fluidmechanik. Springer, Heidelberg

Sinton D (2004) Microscale flow visualization. Microfluid Nanofluid 1(1):2–21

Spies H, Garbe CS (2002) Dense parameter fields from total least squares. In: Van Gool L (ed) Pattern recognition, Lecture Notes in Computer Science, vol LNCS 2449. Springer, Zurich, pp. 379–386

Spies H, Garbe CS, Scharr H, Haußecker H, Jähne B (2004) Flexible regularization schemes. In: Image sequence analysis to investigate dynamic processes. Springer, Berlin

Stone HA, Stroock AD, Ajdari A (2004) Engineering flows in small devices: microfluidics toward a lab-on-a-chip. Annu Rev Fluid Mech 36:381–411

Taylor G (1954) Conditions under which dispersion of a solute in a stream of solvent can be used to measure molecular diffusion. Proc R Soc Lond Ser A 225:473–477

Taylor JA, Yeung ES (1993) Imaging of hydrodynamic and electrokinetic flow profiles in capillaries. Anal Chem 65(20):2928–2932

Terabe S (1989) Electrokinetic chromatography: an interface between electrophoresis and chromatography. TrAC Trends Anal Chem 8(4):129–134

Tsuda T, Ikedo M, Jones G, Dadoo R, Zare RN (1993) Observation of flow profiles in electroosmosis in a rectangular capillary. J Chromatogr A 632(1-2):201–207

Van Huffel S, Vandewalle J (1991) The total least squares problem: computational aspects and analysis. Society for Industrial and Applied Mathematics, Philadelphia

Wang J (2000) From dna biosensors to gene chips. Nucleic Acids Res 28(16):3011–3016

Zhang D, Herbert M (1999) Harmonic maps and their applications in surface matching. In: CVPR'99. Fort Collins, Colorado